symmetry

MDPI

Article

Handed Mirror Symmetry Breaking at the Photo-Excited State of π-Conjugated Rotamers in Solutions

Puhup Puneet [1,*], Sajan Singh [1], Michiya Fujiki [2,*] and Bhanu Nandan [1,*]

[1] Department of Textile and Fibre Engineering, Indian Institute of Technology Delhi (IITD), Delhi 110016, India; ttz158472@textile.iitd.ac.in

[2] Division of Materials Science, Graduate School of Science and Technology, Nara Institute of Science and Technology, 8916-5 Takayama, Ikoma, Nara 630-0036, Japan

* Correspondence: puhuppuneet@textile.iitd.ac.in (P.P.); fujikim@ms.naist.jp (M.F.); nandan@textile.iitd.ac.in (B.N.)

Abstract: The quest to decode the evolution of homochirality of life on earth has stimulated research at the molecular level. In this study, handed mirror symmetry breaking, and molecular parity violation hypotheses of systematically designed π-conjugated rotamers possessing anthracene and bianthracene core were evinced via circularly polarized luminescence (CPL) and circular dichroism (CD). The CPL signals were found to exhibit a (−)-sign, and a handed dissymmetry ratio, which increased with viscosity of achiral solvents depending on the rotation barrier of rotamers. The time-resolved photoluminescence spectroscopy and quantum efficiency measurement of these luminophores in selected solvents reinforced the hypothesis of a viscosity-induced consistent increase of the (−)-sign handed CPL signals.

Keywords: circularly polarized luminescence; circular dichroism; symmetry breaking; parity violation; weak neutral current; rotamer; anthracene; Lippert-Mataga

Citation: Puneet, P.; Singh, S.; Fujiki, M.; Nandan, B. Handed Mirror Symmetry Breaking at the Photo-Excited State of π-Conjugated Rotamers in Solutions. *Symmetry* **2021**, *13*, 272. https://doi.org/10.3390/sym13020272

Academic Editor: Edwin Charles Constable

Received: 12 January 2021

Accepted: 1 February 2021

Published: 5 February 2021

1. Introduction

The fundamental building blocks of life on planet earth are dominated by one of the enantiomer pairs, for instance, L-amino acids and D-sugars. However, they are supposed to be energetically equivalent to another enantiomer and should obey the parity conservation law of mirror symmetry [1–5]. Several theoretical investigations have utilized handed mirror symmetry breaking (MSB) via molecular parity violation (MPV) to explain the natural selection of one enantiomer over the other in biological systems [6–31]. The MPV hypothesis is based on the idea of parity-violating weak neutral current (PV-WNC), owing to the electron–nuclei interaction facilitated by massive neutral Z^0-boson (91 GeV). Consequently, one enantiomer is stabilized slightly in terms of energy by $-E_{pv}$; conversely, the other is destabilized by $+E_{pv}$ and the energy difference is known as the parity-violating weak energy difference (ΔE_{pv}) [7,8,32–34]. Based on the MPV hypothesis, various reports have estimated that the ΔE_{pv} between mirror-image enantiomers is extremely small (10^{-8}–10^{-14} kcal mol^{-1}), which corresponds to the enantiomeric excess (*ee*) of only 10^{-9}–10^{-15} %, i.e., excess of one molecule in the racemic mixture of 10^{11}–10^{17} molecules [14,35,36]. Practically, the detection of such a tiny chiral bias is still a significant challenge owing to the detection limits of conventional spectroscopic methods such as achiral UV-Visible, IR, NMR, ESR, microwave spectrometers and enantioselective column chromatography [37–40]. To make the MPV detectable by spectroscopic measurements, several methods have been postulated to amplify the signals. For instance, linear amplification of faint E_{pv} by the connotation of molecules to polymers and crystals [6], and a small influence of PV-originating oscillation on parity conserving electromagnetic (PC-EM)-originating quantum oscillation of imaginary chiral molecules in a double-well (DW) potential [11]. Additional theoretical models of real and imaginary molecules have been referred to in several innovative re-

ports, along with experimental attempts [6–8,12–14,16–18,20,25–29,41–46]. Recent reports highlight the advance in the realm of MPV [47–50].

Recently, one of the authors (M.F.) and coworkers reported astonishing results from a comprehensive circularly polarized luminescene (CPL) and circular dichroism (CD) spectroscopic data set of nearly fifty non-rigid luminophore rotamers without stereogenic centers [42,43]. On controlling the tunneling barrier (E_b), all these luminophores revealed step-like and consistent alteration in Kuhn's dissymmetry factor (g_{lum}) with only (–)-sign CPL signals with changes in the viscosity of the achiral solvents. They provided a possible explanation for the result, which was that although these non-rigid luminophores are made of lighter atoms possessing non-zero spin–orbit interaction (ζ, kcal·mol^{-1}) [ζ = 0.1 (C), 0.2 (N), 0.4 (O), 0.7 (F), 1.0 (S)], a large number of photoexcited luminophores (>10^{10}–10^{16}) confined in a cuvette interacted with focused incident light beams. Subsequently, the faint ΔE_{pv} on the order of 10^{-8}–10^{-14} kcal·mol^{-1} was resonantly amplified to a detectable level to produce CPL chiroptical signals during a synchronized spontaneous radiation process [43]. The authenticity of the results were verified by studying luminophores with an enantiomeric chiral center and achiral D_{2h}-symmetric fused aromatics (naphthalene, anthracene, tetracene, and pyrene). The mirror-image CPL and CD spectra were observed for the luminophores with chiral centers, whereas no detectable CPL and CD spectra were observed for the rigid fused aromatics.

CPL spectroscopy may be a promising tool to experimentally observe molecular parity violation effects:however, a moredetailed theoretical understanding and experimental investigations are requiredto understand the relationships between MPV with (–)-sign g_{lum}, photodynamics, quantum efficiency, and solvent viscosity. Moreover, it is not yet known whether this approach is consistent with other synthetic π- molecular and polymeric rotamers associated with different directions (horizontal and/or vertical) of π-conjugation and rotational barriers.

Based on previous reports [42,43], we rationally synthesized three non-rigid extended π-conjugated luminophores. These luminophores consist of anthracene (single horizontal and verticle conjugation axis), bis-anthracene (single horizontal and double vertical conjugation axes), and biphenyl moieties (single horizontal conjugation axis) as twistable cores in the right- or left-hand geometries, which commonly carry two floppy *trans*-styryl moieties as labile pendants that provide excellent solubility to a broad range of organic solvents. These rotamers possess different rotational barriers that were tunable with the apparent viscosity of achiral solvents, resulting in alterations in chiroptical spectroscopic response. More importantly, handed MSB phenomena was evinced by (–)-sign g_{lum} associated with no dominant CD signals for luminophores dissolved in a series of achiral alcohols. For a comprehensive study, we comparedthe obtained similar (–)-sign CPL signals of an unsubstituted twistable bi-aryl compound and chain-like π-conjugated polymer in solutions. Subsequently, the MPV effect of these luminophores observed by CPL spectroscopy was complemented by time-resolved photoluminescence spectroscopy (TRPL), relative quantum efficiency (Φ_f) measurements and change in dipole moment. The photophysical and chiroptical properties predicted by density functional theory (DFT) and time-dependent DFT (TD-DFT) calculations of luminophores consistently supported the experimental observations.

2. Materials and Methods

2.1. Synthesis and Characterization of Luminophores

Synthesis of 4,4′-distyryl-1,1′-biphenyl (**DSA**): this was synthesized according to the literature [50]. 9,10-Dibromobianthracene (200 mg, 0.595 mmol), styrene (148 mg, 1.428 mmol), K_3PO_4 (0.63 g, 2.975 mmol), and $Pd(OAc)_2$ (26.7 mg, 0.119 mmol) were dissolved in dry dimethylacetamide (40 mL). The reaction mixture was heated to 110 °C and stirred for 24 h. The hot reaction mixture was allowed to cool to room temperature, then it was poured into water. The crude product was extracted twice with $CHCl_3$ (60 mL) and the combined organic extracts were dried over Na_2SO_4. The solvent was evaporated

to 5 mL; the product crystallized after addition of hexane and isolated as a yellow solid (40% yield).

Synthesis of 10,10′-distyryl-9,9′-bianthracene (**DSBA**): 10,10′-Dibromo-9,9′-bianthracene (200 mg, 0.39 mmol), styrene (97 mg, 0.93 mmol), K_3PO_4 (0.41 g, 1.95 mmol), and $Pd(OAc)_2$ (17.5 mg, 0.078 mmol) were dissolved in dry dimethylacetamide (40 mL). The reaction mixture was heated to 110 °C and stirred for 24 h. The hot reaction mixture was allowed to cool down to room temperature, then it was poured into water. The product was extracted twice with $CHCl_3$ (60 mL) and the combined organic extracts were dried over Na_2SO_4. The solvent was evaporated to 5 mL; the product crystallized after addition of hexane and isolated as a yellow solid (45% yield). ^{1}H-NMR (δ in ppm 400 MHz, $CDCl_3$): 8.55 (*d*, 4H, ArH), 8.13 (*d*, 4H, ArH), 7.81 (*d*, 4H, ArH), 7.54 (*m*, 4H, ArH), 7.45 (*m*, 8H, ArH), 7.19 (*s*, 4H, CH=CH), 7.14 (*s*, 2H, ArH). M/z = 558.41 g/mol (MALDI-TOF).

Synthesis of 4,4′-distyryl-1,1′-biphenyl (**DSBP**): 4,4′-Dibromo-1,1′-biphenyl (200 mg, 0.64 mmol), styrene (160 mg, 1.53 mmol), K_3PO_4 (0.68 g, 3.2 mmol), and $Pd(OAc)_2$ (28.8 mg, 0.12 mmol) were dissolved in dry dimethylacetamide (30 mL). The reaction mixture was heated to 110 °C and stirred for 24 h. The hot reaction mixture was allowed to cool down to room temperature, then it was poured into water. The product was extracted twice with $CHCl_3$ (60 mL) and the combined organic extracts were dried over Na_2SO_4. The solvent was evaporated to 5 mL; the product crystallized after addition of hexane and isolated as a solid (29 % yield). ^{1}H-NMR (δ in ppm 400 MHz, $CDCl_3$): 7.66 (*d*, 4H, ArH), 7.62 (*d*, 4H, ArH), 7.57 (*d*, 4H, ArH), 7.40 (*t*, 4H, ArH), 7.30 (*m*, 2H), 7.18 (*s*, 4H, CH=CH). M/z = 358 g/mol (Maldi-tof).

2.2. Preparation of Sample Solutions

First, a stock solution of luminophore (10^{-3} M) was prepared in a suitable organic solvent. For **DSA** and **DSBA**, chloroform was used as the stock solution as solvent, and for **DSBP**, methanol was used as a stock solution as solvent. Premeasured aliquots of stock solution were added to 1.9–2.1 mL of the desired liquid in a cylindrical quartz cuvette using a micro-syringe and diluted with a range of solvents followed by vigorous shaking by hand to minimize the incorporation of external (chiral) dust, fiber, particles. It was confirmed that the mixed solution was a scattering-free, transparent homogeneous solution before the CD and CPL measurements.

2.3. Instrumentation

Simultaneous measurements of CD and UV-visible spectra were done at room temperature using a cylindrical quartz cuvette with path lengths of 10 mm (JASCO J-820 spectropolarimeter, Hachioji, Tokyo, Japan). The cylindrical cuvette appears to provide precise CD measurements as compared to rectangular cuvettes. To ensure reliability, one or two accumulations of the spectra were recorded. Similarly, simultaneous measurements of CPL and PL spectra were performed on a JASCO CPL-200 spectrofluoropolarimeter using cylindrical quartz cuvettes at room temperature. The reliability of the measurements was ensured by recording two to three accumulations of spectra.

The NMR spectra were measured with a Bruker-400 MHz; the mass spectra were measured with a Bruker (Bengaluru, Karnataka, India) UltrafleXtreme MALDI-TOF/TOF mass spectrometer; luminescence lifetime decay was recorded with time correlated single photon counting (TCSPC) using Edinburgh Instruments (Kirkton Campus, Livingston, UK) FLSP920 time-resolved fluorescence spectrometer. A pulsed laser diode (377 nm) with a pulse repetition rate of 500 kHz was employed for the mean lifetime measurements.

3. Results

DSA, **DSBA,** and **DSBP** (Chart 1) were synthesized according to Section 2.1. For comparison, we investigated two commercial rotamers, including 9,9′-bianthracene (**BA**) and poly{[2,5-bis(2-(N,N-diethylammoniumbromide)ethoxy)-1,4-phenylene]-alt-1,4-pheynlene (**PP**) (Chart 1). **BA** is a core moiety of **DSBA** and **PP** is regarded as an extension of multiple

cores in **DSBP**. The CPL and CD spectra of all luminophores were measured in a series of linear alkane mono-ols and diols with different viscosities at 25 °C, ranging from 0.59 cP and 7.0 cP. The CPL signals for all the three luminophores were of (−)-sign, which kept on increasing in relation to the viscosity of the solvent, whereas they remained CD-silent irrespective of the viscosity of the solvent. The non-aggregated molecular conformations of these molecules were investigated in this study by performing chiroptical measurements in dilute solutions (10^{-6}–10^{-5} M). However, if we consider the optical properties of **DSA,** for instance, and compare it with the predicted UV-Visible spectra of cis-**DSA** and trans-**DSA** during CD and CPL measurements (Figure S15, Supplementary Material (SM)), it is difficult to determine whether cis or trans isomer is involved. An experimental observation indicated there was a transoid–cisoid conformational transition arising from the rapid rotational transition of two labile styryl groups.

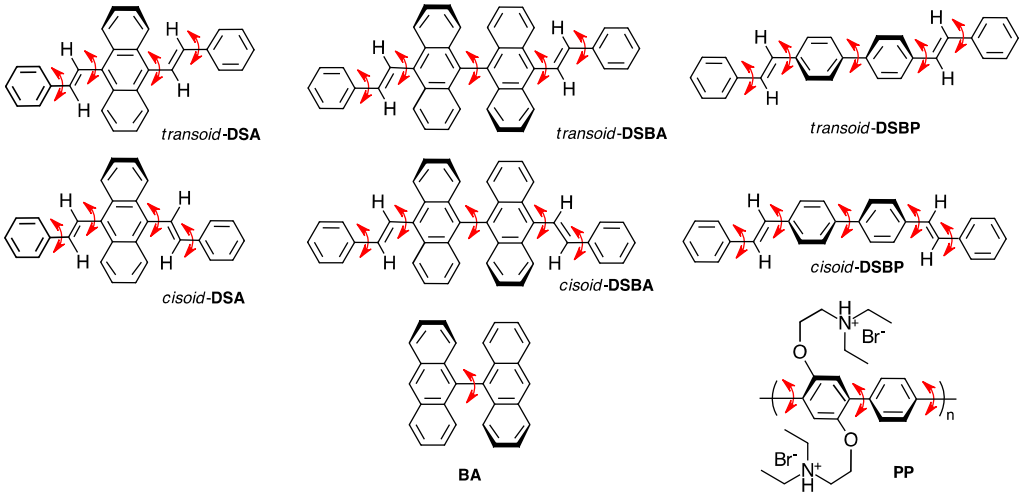

Chart 1. Chemical structure of luminophore rotamers. The arrow in red represents the labile rotation axis. **DSA**, **DSBA**, and **DSBP** show less-polar *transoid* and polar *cisoid* vinylic conformers.

3.1. Chiroptical Properties

3.1.1. **DSA**

In the case of **DSA**, the CPL profile (g_{lum}) observed in methanol and 1,4-butanediols were compared. The signal intensity was much higher in 1,4-butanediol ($g_{lum} = -1.7 \times 10^{-3}$) as compared to that in methanol ($g_{lum} = -0.5 \times 10^{-3}$) (Figure 1a). Also, the CPL–viscosity plot shows a cluster of data points for g_{lum} for lower viscosity solvents, an increasing tendency for higher viscosity solvents and becomes nearly constant with viscosity of more than 33 cP (Figure 1d). This behavior can be attributed to the labile flip-flop motion of the π-extended styryl group until the media is sufficiently viscous. Once the rotational freedom was fully restricted due to molasses in the media, **DSA** molecules adopted a time-averaged stable conformation, which revealed mainly (–)-sign CPL signals. Anomalous behavior was observed in the emission properties of **DSA** in the diols, where a significant blue shift was observed along with intense CPL signals. The observed blueshift may occur, possibly, due to the formation of an intermolecular OH-π adduct of **DSA** with diol molecules. It distorted the rotational degree of styryl units. Hence, the extension of π-conjugation was moderated. As a result, emission phenomenon approaches a blue-shifted anthracene type behavior.

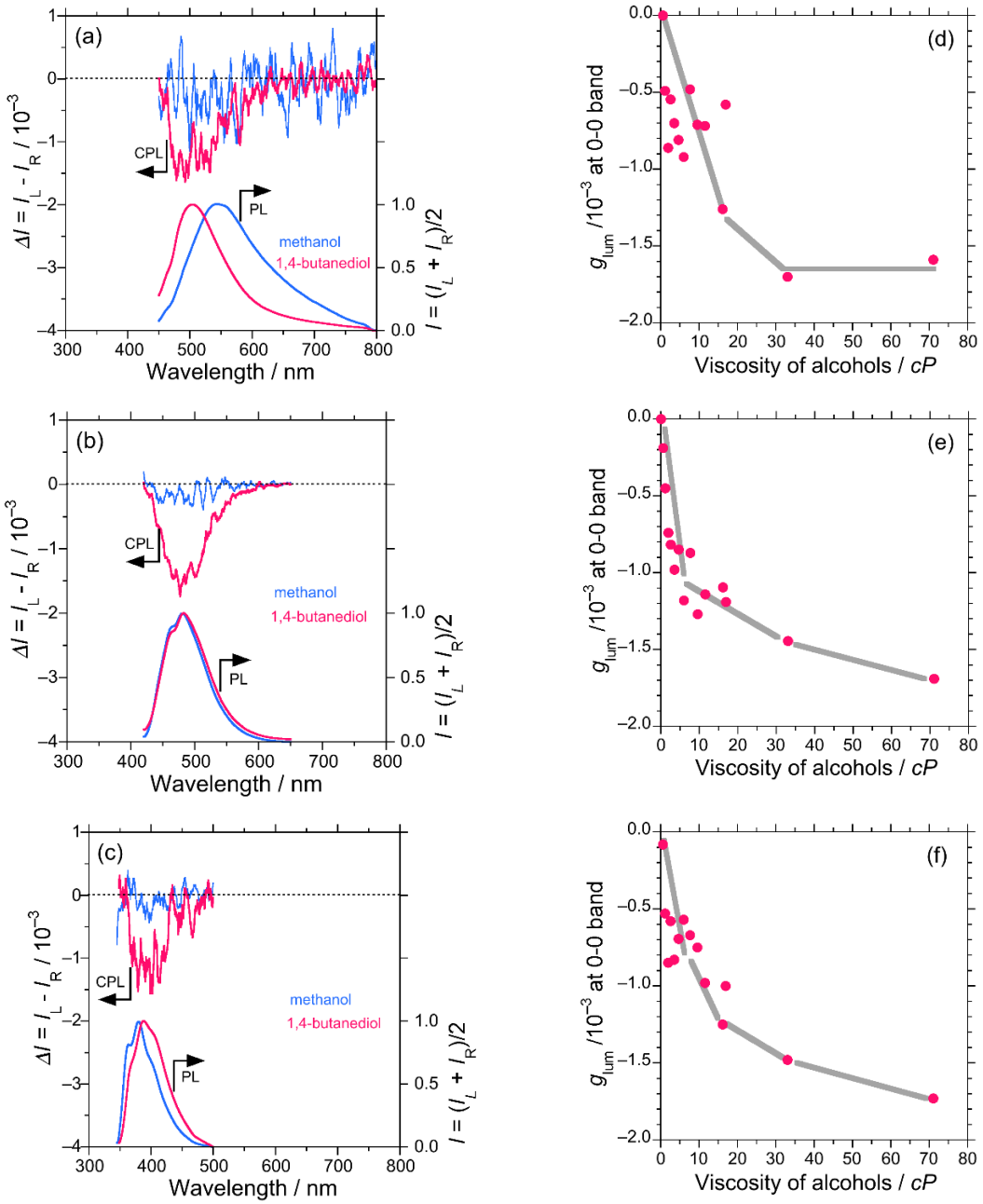

Figure 1. Comparison of the CPL and photo-luminescence (PL) spectra in methanol and 1,4-butanediol for **DSA** excited at 420 nm (**a**), **DSBA** excited at 390 nm (**b**), and **DSBP** excited at 320 nm (**c**). The g_{lum} values at 0-0 PL band extremum of **DSA** (**d**), **DSBA** (**e**), and **DSBP** (**f**) as a function of the viscosity of alcohol, respectively: methanol (0.55 *cP*), ethanol (1.09 *cP*), *n*-propanol (1.96 *cP*), *n*-butanol (2.59 *cP*), *n*-pentanol (3.47 *cP*), *n*-hexanol (4.59 *cP*), *n*-heptanol (5.97 *cP*), *n*-octanol (7.59 *cP*), *n*-nonanol (9.51 *cP*), *n*-decanol (11.50 *cP*), ethylene glycol (16.1 *cP*), *n*-undecanol (16.95 *cP*), 1,3-propandiol (33.0 *cP*), and 1,4-butanediol (71.0 *cP*) [42,43].

3.1.2. **DSBA** and **BA**

DSBA possesses a bianthracene core and owing to an inherent substantial intramolecular steric hindrance, **DSBA** remains at a twisted angle of (90.07°) with D_{2h}-like molecular symmetry or exact D_2-symmetry based on an optimized structure by DFT calculations (Table S6 in SM). This geometry of the molecule should not display any obvious CPL signal owing to the nearly achiral D_{2h}-like symmetry of the core. The photoluminescence (PL) spectra showed two emission bands, namely, 0-0 and 0-1 vibronic bands. As the viscosity of the media increased, the (–)-sign CPL signal at the 0-0, 0-1 vibronic bands increased con-

sistently (Figure 1d,e). Figure 1b demonstrates the CPL profile and stronger CPL intensity in more viscous 1,4-butanediol ($g_{lum} = -1.7 \times 10^{-3}$) as compared to less viscous methanol ($g_{lum} = -0.3 \times 10^{-3}$). This result infers that the viscous medium enforces the molecular rotation of the bianthracene core more significantly as compared to **DSA,** owing to the relatively high rotational barrier height of the bianthracene core. Since most of the PL and CPL signals of **DSBA** come from the bianthracene core, the effect of the OH/π-interaction with diols was not observed. To support the hypothesis of viscosity dependent twisting of the bianthracene core, **BA** was examined through CD and CPL measurements. Similar to the case of **DSBA**, the chiroptical properties of **BA** in methanol, ethanol, and 1-propanol exhibited a linear increase in the (–)-sign CPL signal with an increase in the viscosity of the solvents (Figure S14, SM).

Moreover, theoretical calculations were employed for **BA** with a forced twist angle as a function of the dihedral angle between two anthracene units ranging from 30° and 90°. In the case of **BA**, the ground state energy increased exponentially with a decrease in twist angle (Figure S13, SM). This implies that one has to raise the ground state energy of **BA** to achieve a smaller twist angle, which no longer remains in the pseudo-D_{2h}-symmetry. Thus, **BA** can adopt a time-averaged right (*R*)- or left (*L*)-state. In this study, we achieved mechanical twisting of **BA** and the bianthracene core of **DSBA** with an enhancement in the viscosity of the solvent.

3.1.3. **DSBP** and **PP**

DSBP possesses a built-in twisted biphenyl core owing to its inherent intra-molecular twisting capability. **DSBP** revealed a similar consistent increase in the (–)-sign CPL signal with the viscosity of the solvent at two vibronic bands in PL and CPL (0-0 and 0-1) spectra (Figure 1c–f).

For additional comparison, we measured the chiroptical properties of **PP**, which is an oligomer with several phenylene units. The oligomer **PP** showed an intense (–)-sign CPL signal, even in a very low viscous methanol. In higher viscosity solvents, the (–)-sign CPL signal appeared to have saturated, and a negligible effect on CPL intensity was observed (Figure S14, SM). Hence, a high degree of polymerization of π-conjugated units is assumed to have a similar effect as luminophores in the highly viscous environment due to the long chains and their sluggish movements. Moreover, the intense CPL signals can be accredited to enhanced π-conjugation along the main chain, whereas (–)-sign signal is maintained because of the handed conformation locked by the long main-chain lengths.

3.1.4. Mean Excited-State Lifetime and Relative Quantum Efficiency of DSA, DSBA and DSBP

It is commonly understood in chemistry that molecules in the photoexcited state lose energy via a non-radiative decay channel. In principle, the non-radiative loss can be curbed if molecular rotational and vibrational modes are restricted in viscous solvents [48,49]. To collect more evidence on the parity-violating (–)-sign CPL enhancement with the viscosity of the solvent, the mean excited state lifetime (τ)of luminophores and relative Φ_f were measured as a function of viscosity in selected solvents (ethanol = 1.19 *cP* (25 °C), *n*-pentanol = 3.47 *cP* (25 °C), *n*-octanol = 7.59 *cP* (25 °C), and *n*-undecanol = 16.95 *cP* (25 °C)).

The τ values for **DSA**, **DSBA**, and **DSBP** reduced linearly with an increase in the viscosity of the solvent (Figure 2b). This signifies that the excitons emit faster, which is associated with a lesser probability of non-radiative decay in a viscous environment. Similarly, the relative Φ_f showed an increasing tendency for **DSA** and **DSBA**, whereas it remained almost constant with slight fluctuations for **DSBP** (Figure 2b and Tables S3–S5, SM). Using these values, the rate of radiative decay (K_f) was calculated ($K_f = \Phi_f/\tau$). The profile of K_f vs. τ exhibited a linear decreasing trend, and K_f vs. Φ_f showed an increasing trend (Figure 2a) of **DSA**, **DSBA,** and **DSBP**. The K_f value for **DSA** and **DSBA** showed an increasing tendency with the viscosity of the solvent, whereas the K_f value for **DSBP** remained almost constant with slight fluctuations (Figure 2c). This implies that the τ,

Φ_f, and K_f values are complementary to the intensified characteristics of parity-violating handed CPL signals along with time-averaged handed conformation of luminophores in a DW for **DSA** and **DSBA**. In the case of **DSBP**, no significant increasing tendency was observed for Φ_f and K_f, however, a consistent decreasing trend of τ suggests that the CPL signals intensify with an increase in the viscosity of the solvent.

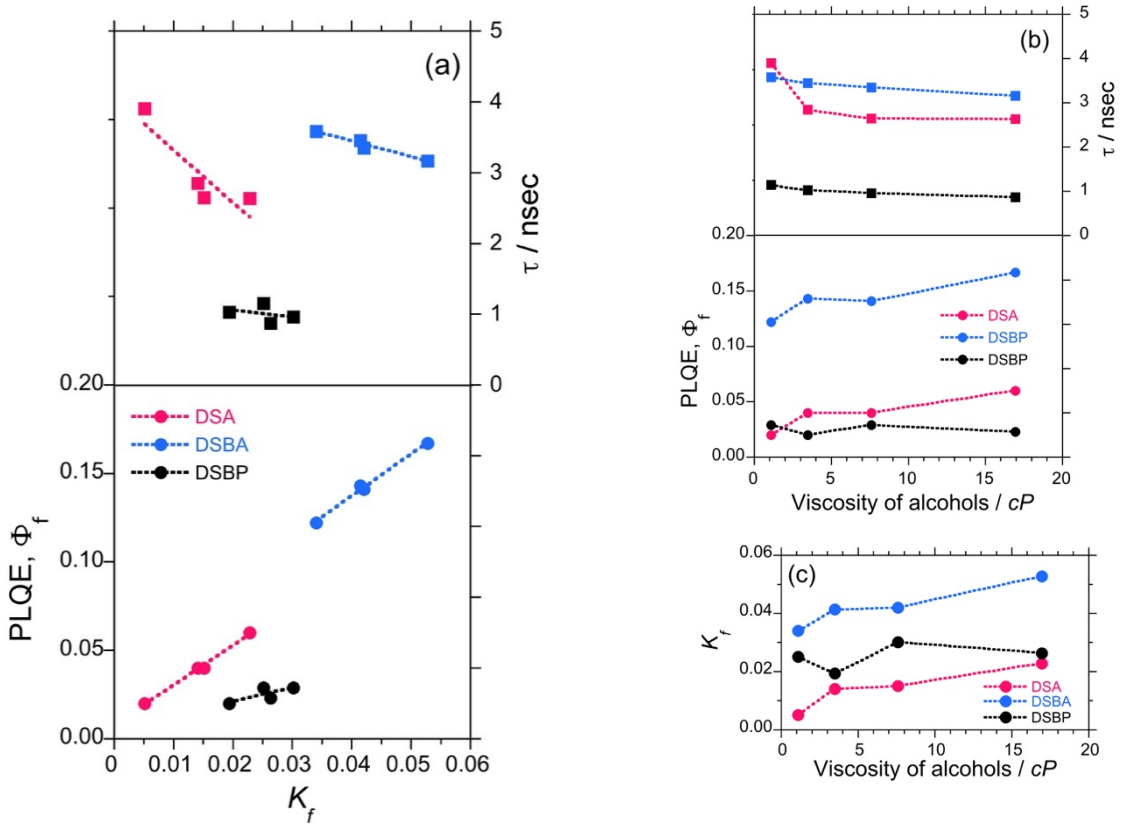

Figure 2. Relationships between radiative decay rate (K_f), photoluminescence lifetime (τ), and quantum yield (Φ_f) of **DSA** (red filled circles and squares), **DSBA** (blue filled circles and squares), and **DSBP** (black filled circles and squares) (**a**), the relationship between Φ_f, τ and the viscosity of four alcohols (**b**), and the relationship between K_f and the solvent viscosity (**c**). The solvents are ethanol 1.19 *cP* (25 °C), *n*-pentanol 3.47 *cP* (25 °C), *n*-octanol 7.59 *cP* (25 °C), and *n*-undecanol 16.95 *cP* (25 °C)) [48,49].

3.1.5. Changes in Dipole Moment and Theoretical Calculations

The change in dipole moment $\Delta\mu$ (= $\mu_e - \mu_g$) was calculated according to the literature [51,52] (Section 5, SM). In the case of **DSA** and **DSBA**, their $\Delta\mu$ values were found to be 9.66 D and 7.74 D, respectively. The change in dipole moment in the excited state as compared to the ground state is directly correlated to the nature of the luminophore in the excited state and its intramolecular charge transfer state. Such a high $\Delta\mu$ for **DSA** and **DSBA** strongly supports the presence of a twisted intramolecular charge-transfer state (TICT) in the excited state. The twisting of luminophores caused them to have a higher polarity in the excited state, which ultimately resulted in the high $\Delta\mu$ values. Contrarily, the $\Delta\mu$ value of **DSBP** was 2.79 D, which is moderate compared to **DSA** and **DSBA**; however, experimentally, we still observed dominant CPL signals with an increase in viscosity of the solvent. These behaviors can be explained by the DFT-optimized structure and HOMOs-and-LUMOs of luminophores. The **DSA** and **DSBA** possess anthracene and bianthracene cores, respectively, which contribute to the vertical conjugation (longer axis of the anthracene ring) along with the horizontal conjugation (shorter axis of the ring). Hence, TICT is more dependent on the twisting of anthracene and bianthracene core [53].

In the case of **DSBP**, because only the horizontal conjugation is possible, the TICT does not dominate to yield the high $\Delta\mu$ value. The CPL measurements are more sensitive, hence, the $\Delta\mu$ value of 2.79 D appeared to produce sufficiently large CPL signals.

Theoretical calculations were also performed to investigate the properties of the luminophores at several intramolecular twisted states. The **DSA** possesses a stable anthracene core but two twistable styryl groups at each end. These two variables would significantly increase the number of twisted states. For simplicity, we omitted such calculations. The twisted states of **DSBP** containing biphenyl core were generated hypothetically by varying the dihedral angles of the biphenyl core from 5°–90° with an interval of 5°, while keeping the dihedral angle of the styryl groups as optimized (~53°). By employing these structures, single-point energy calculations were performed using DFT and TD-DFT (B3LYP, 6-311G). The plots of energy at the ground state (GS) and excited state (ES) vs. the dihedral angle of biphenyl core reveals that, although **DSBP** at GS remains with a dihedral angle of 39°, **DSBP** adopts a conformation with a dihedral angle of ~15° at the ES (Figure 3a). Such an extensive twisting capability is correlated with small rotational barriers (1–2 kcal mol^{-1}) for the biphenyl group at GS and ES. As a result, the molecule is expected to lose absorbed photoexcited energy by non-radiative decay pathways.

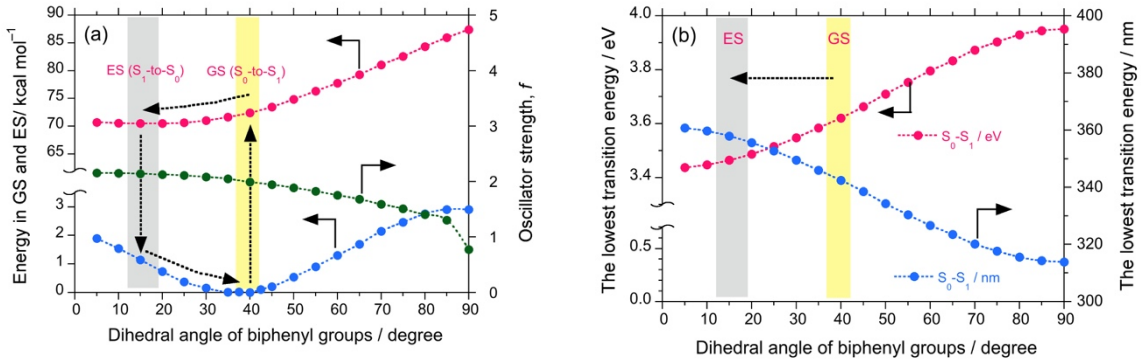

Figure 3. The calculated energy (DFT/TD-DFT, B3LYP, 6-311G) for **DSBP** at GS (blue filled circles) and ES (red filled circles) and oscillator strength (green filled circles) as a function of dihedral angle of biphenyl groups (**a**). The lowest transition energy (left-side ordinate in eV, red filled circles and right-side ordinate in nm, blue filled circles) as a function of dihedral angle of biphenyl groups (**b**).

Correspondingly, the estimated oscillator strength (f) showed a slight increase from 2.07 at GS to 2.15 at ES, which can be directly correlated with the Φ_f values. These results infer that **DSBP** at ES adopts a stable handed conformation with a dihedral angle of ~15°. This arises from the small energy barrier of rotation and loss of photoexcited energy as a non-radiative decay pathway, even in fluidic viscous solvents. Such an energy loss coupled with a slight increase in f value results in almost constant values of Φ_f and K_f ($K_f = \Phi_f/\tau$). However, the consistent increase of (–)-sign CPL signals is attributed to the decrease of τ value associated with an increase of viscosity of the solvent. Moreover, the deeper energy well with the dihedral angle at GS and moderately deep energy well at ES suggest appreciable tunneling through the energy barrier to adopt a right-handed conformation, which is a one-way route for the excitons because of slight stabilization of the right-hand state by ΔE_{pv}.

Further, the plot of the dihedral angle vs. the lowest transition energy (eV, nm) reveals a change in the lowest transition energy from 3.54 eV (349 nm) at GS to 3.39 eV (362 nm) at ES, which also complements the experimental observations of a large Stokes shift (from 330 nm to 393 nm, ~4850 cm^{-1} or 0.60 eV) (Figure 3b). Similarly, **DSBA** possesses a bianthryl core; its twisted states were generated hypothetically by varying the dihedral angles of bianthryl core from 30°–90° with an interval of 5° while keeping the dihedral angle of styryl groups optimized (~53°). By employing these twisted structures, single-point energy calculations were performed using DFT and TD-DFT (B3LYP, 6-311G).

The plots of energy at GS and ES as a function of the dihedral angle of biphenyl core revealed that **DSBA** remains at GS with a dihedral angle of 90.07° and subsequently adopts a conformation with a dihedral angle of ~80° at ES. The energy profile reveals a much higher energy barrier for intra-molecular rotation as compared to **DSBP**, which increased exponentially with a decrease in the dihedral angle of bianthryl core. Therefore, only a small intra-molecular reorganization could be observed from GS to ES (Figure 4a). Further, the f value as a function of the dihedral angle showed an increase in f from GS (0.00079) to ES (0.04063) owing to the small intra-molecular reorganization due to a large rotational barrier (Figure 4b). As a result, when the viscosity of the solvent was increased, consistent increases in Φ_f and K_f values of **DSBA** were observed, associated with the decrease in τ value. This tendency is significantly supported by the corresponding (–)-sign CPL signals.

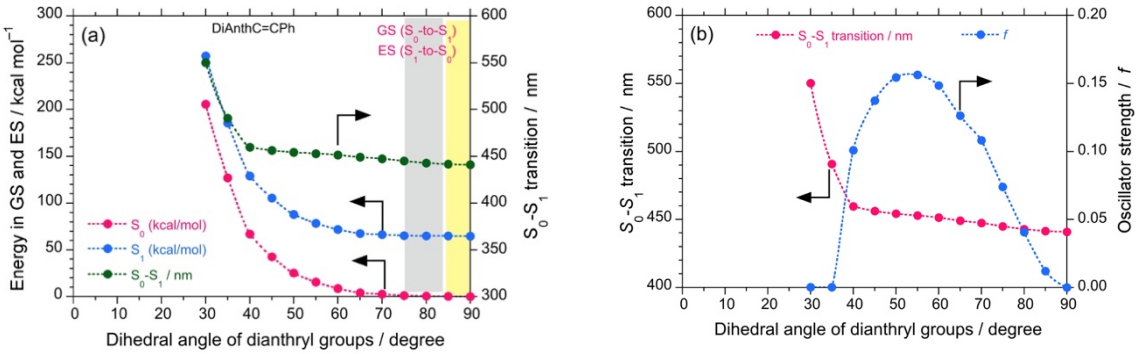

Figure 4. The calculated energy, S_0-S_1 (in kcal mol^{-1}, green filled circles) obtained with DFT/TD-DFT, B3LYP, 6-311G) for **DSBA** at GS (red filled circles) and ES (blue filled circles) as a function of the dihedral angle of bianthryl groups (**a**). The S_0-S_1 transition (in nm, red filled circles) and oscillator strength (f, blue filled circles) as a function of the dihedral angle of bianthryl groups (**b**).

Additionally, to ensure the authenticity of the experimentally observed (–)-CPL signals of the luminophores, we predicted CD spectra at GS and ES with the corresponding dihedral angles of biphenyl and bianthryl core by performing DFT/TD-DFT calculations (Figure 5). The predicted CD spectra at ES corresponds to CPL signals. In the case of **DSBP**, the predicted CD spectra at both GS and ES showed a significant (–)-sign Cotton band with comparable intensities. The similar intensity at GS and ES also complements the anomalous behavior of **DSBP**, i.e., the minimal increase in f and loss of energy via intra-molecular reorganization (Figure 5b). Conversely, for **DSBA**, a significant (–)-sign Cotton band was observed at GS, whereas a lot of intense signal was observed at ES owing to the intramolecular twisting and subsequent increase of Φ_f and f (Figure 5a). These predicted CD spectra indisputably support the experimental observations.

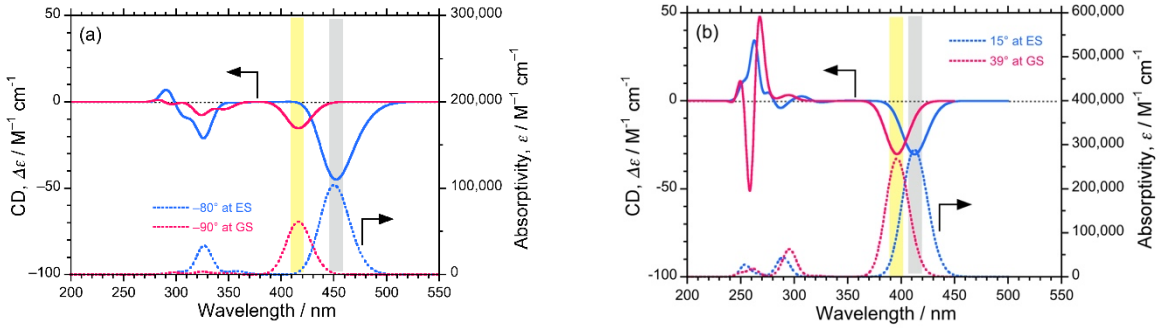

Figure 5. The predicted CD (top) and UV-visible (bottom) spectra of **DSBA** (**a**) and **DSBP** (**b**) at GS (red lines) and ES (blue lines).

4. Discussion

The experimental observation of variation in g_{lum} for luminophores in relation to the viscosity of the solvent is evident from Figure 1, indicating handed MSB via MPV. The systematic study of critical photophysical properties such as τ, Φ_f, and K_f, revealed the photodynamics of luminophores at the excited state, which could be significantly modulated with changes in the viscosity of the media (Figure 2), whereas $\Delta\mu$ depended on the presence of TICT (Section 5, ESI). Consequently, variations in GS and ES energy with dihedral angle predicted by DFT calculations supported the hypothesis of viscosity-dependent rotational freedom (Figures 3 and 4). It is known that viscosity of the solvent can be directly correlated with the quantum tunneling energy barrier (E_b) of left- and right-handed states of chiral molecules [26,42], thus, one can speculate that rotamers studied here exhibit variation in handed chiroptical signals via variations in E_b. However, one can still be skeptical about the experimental observation of such as small bias in MSB via MPV, and a suitable theoretical model should be adopted that builds on several theoretical treatments and models. According to the theoretical treatment suggested by Hegstorm and McDermott [42], Quack et al. [27], and Bargueño [28], the chiral bias of eigenstates of chiral forms of molecules $\Psi_{(\pm)}$, is given by $\cos^2\beta - \sin^2\beta = \cos 2\beta$, where β is the mixing angle ranging 0° to 45° and

$$\cos 2\beta = \frac{\Delta E_{\mathrm{pv}}}{\sqrt{(\Delta E_{\mathrm{pv}})^2 + \delta^2}} \approx \frac{\Delta E_{\mathrm{pv}}}{\delta} \quad (1)$$

where δ is half of the tunneling splitting ($\Delta E_{\pm}$).

(i) In the case of molecules delocalizing rapidly between the left-handed and right-handed states, we have $\Delta E_{\pm} >> \Delta E_{\mathrm{pv}}$, giving $\beta \rightarrow 45°$. Hence, $\cos\beta = \sin\beta = (1/\sqrt{2})$, which allows one to recover the parity eigenstates $\Psi^{(\pm)}$.For example, ammonia-like molecules remain in a superposition of left-handed and right-handed states because the tunneling time is in milliseconds.

(ii) Molecules exhibiting stable handed forms have $\Delta E_{\mathrm{pv}} >> \Delta E_{\pm}$, giving $\beta \rightarrow 0$. In this case, the energy eigenstates tend to become handed states, for example, biomolecules with stable chiral states.

(iii) Other molecules that form the subject of the current study have ΔE_{pv} and $\Delta E_{\pm}$ that are comparable in magnitude. These molecules would remain in a superposition but with a minor and measurable bias to one side, of the order $\cos 2\beta$.

For a typical polyatomic molecule with a ΔE_{pv} of 10^{-16} kT, and a $\Delta E_{\pm}$ of the order 10^{-10} kT, we get $\Delta E_{\mathrm{pv}}/\delta = 10^{-6}$. With this insight, instead of looking at the very weak $\Delta E_{pv}/kT$, which employs the measurement of differences in the enantiomeric population based on Boltzmann distribution, one can measure $\Delta E_{\mathrm{pv}}/\delta$, which should possibly be measured by commonly employed spectropolarimeters. The notable examples are Faraday polarimeters to measure the electroweak optical rotation of atoms and cavity ring-down polarimeters for selected molecules. Hegstorm and McDermott further argue that any molecular property P exhibiting opposite sign for enantiomers would behave as

$$P\pm = \mp P_1 \cos 2\beta \quad (2)$$

In relation to the theoretical treatments presented above [27,28,42], Bouchiat et al. estimated theoretically that the degree of circular polarization of cesium vapor, lead vapor, and molecular oxygen gas, arising from parity-violating weak neutral current (WNC) is mediated by massive neutral Z^0 boson (91 GeV) [54]. Actually, physicists have succeeded in measuring an optical rotation dispersion (ORD) spectrum of atomic lead vapor at 1240 nm as an absorption mode [50]. Moreover, Quack has proposed a method for the preparation of molecules in well-defined parity states, evolving with time and selective probing to an electronic excited state [54]. Later, Berger suggested a comprehensive method to probe molecules that are achiral at the ground state ($\Delta E_{\pm} >> \Delta E_{\mathrm{pv}}$) but due to the influence of parity violating potential in the excited state may acquire opposite parity [55]. This method

also predicts the possibility of a smaller tunneling splitting barrier at excited states (smaller $\Delta E_{\pm}$), which would be comparable to parity violating energy, i.e., $\Delta E_{\pm} \sim \Delta E_{\mathrm{pv}}$. Further, this approach may not only improve the ability to measure the magnitude of ΔE_{pv}, but also widens the possible designs of realistic molecules that can be probed with electronic excitation. An emerging spectroscopic technique to study the effect of chirality in electronic excited states of the molecules is circularly polarized luminescence (CPL) spectroscopy). Notably, Bouchiat's team detected a high-resolution PL-detective CD spectrum of cesium vapor by monitoring a near-infrared emission ($6P_{1/2}$–$7S_{1/2}$ transition at 1360 nm) upon circularly polarized photoexcitation of forbidden $6S_{1/2}$–$7S_{1/2}$ transition at 539 nm [56]; similar to the fluorescence-detective circular dichroism spectroscopy, the so-called FD-CD technique that is equivalent to the present technique.

Based on the theoretical predictions, followed by the experimental attempts discussed above, one can hypothesize that experimental detection of MPV may be possible when proper luminophore rotamers with $\Delta E_{\mathrm{pv}} \sim \Delta E_{\pm}$ are employed under carefully controlled conditions at ambient temperature, using the state-of-the-art CPL and CD spectropolarimeters.

Thus far, several experimental studies have validated the MSB hypothesis in the quest to understand the differences in physical and optical properties of enantiomeric compounds [53,57–61]. With regard to the linear amplification model and the phase transition models at the far-from-equilibrium, when large numbers (>10^{10}–10^{16}) of enantiomeric luminophores are photoexcited macroscopically in a chorus to the first excited S_1 state, the extreme small *ee*, and feeble ΔE_{pv} may be greatly enhanced to a detectable level. It is understood that, in the case of enantiomeric rotamers in a symmetrical DW at the S_1 state, the enantiomers may promptly oscillate between *L*- and *R*-states with time; subsequently time-averaged CPL signals are produced. Moreover, if enantiomers of rotamers with time are considered in dissymmetrical DW at the S_1 state, they may favor a one-way route via quantum tunneling, mediated by a weak neutral current mediated by Z^0 boson.

Figure 6 illustrates a system that is achiral at the ground state ($\Delta E_{\pm} >> \Delta E_{\mathrm{pv}}$) but due to the influence of parity-violating potential at the electronic excited state, may acquire inversed parity, which can be probed by radiative decay. This scenario led us to assume that only (+)- or (–)-sign CPL signals could be detectable via handed rotational and flip-flop motions.

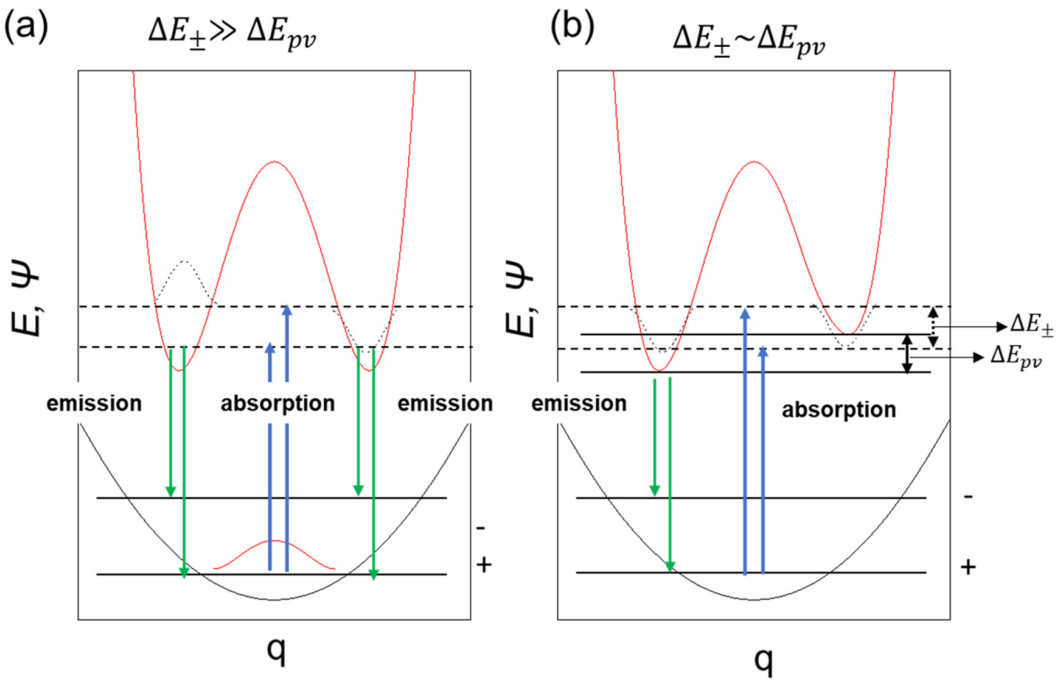

Figure 6. A schematic model of symmetrical double-well (**a**) and dis-symmetrical double-well in the photoexcited state (**b**) coupled with single well in the ground state.

5. Conclusions

Regarding the MPV hypothesis, we collected comprehensive experimental data from photoexcited MSB for three non-rigid π-conjugated rotamers (**DSA**, **DSBA**, and **DSBP**), and for comparison, **BA** and **PP** using CPL spectroscopy. **DSA**, **DSBA**, and **DSBP** carrying two floppy styryl groups were rationally designed and synthesized. The values of τ and Φ_f in selective solvents were obtained, followed by the calculated K_f value, which agreed with an enhanced radiative decay process when the viscosity of the solvents increased. Several theoretical calculations, including the effect of solvent viscosity on the τ and Φ_f [52] values provided new insight into the behavior of these luminophore rotamers at GS and ES and complemented all the present experimental observations. Our findings offer experimental templates for rationally designing non-rigid π-conjugated molecules [62], polymers, and supramolecules [50] as luminophores rotamers at ES to detect similar MPV effects, revealing only (–)-sign CPL signals and/or non-mirror-image CPL spectra, as mentioned above.

Supplementary Materials: The following are available online at https://www.mdpi.com/2073-8994/13/2/272/s1, Figure S1: ^{1}H-NMR spectrum (a) and MALDI-TOF spectrum (b) of **DSBA**; Figure S2: ^{1}H-NMR spectrum (a) and MALDI-TOF spectrum (b) of **DSBP**; Figure S3: CPL spectra of **DSA** in methanol (a), ethanol (b), *n*-propanol (c), *n*-butanol (d), *n*-pentanol (e), *n*-hexanol (f), *n*-heptanol (g), *n*-octanol (h), *n*-nonanol (i), *n*-decanol (j), *n*-undecanol (k), ethyleneglycol (l), 1,3-propanediol (m), 1,4-butanediol (n); Figure S4: CD spectra of **DSA** in methanol (a), ethanol (b), *n*-propanol (c), *n*-butanol (d), *n*-pentanol (e), *n*-hexanol (f), *n*-heptanol (g), *n*-octanol (h), *n*-nonanol (i), *n*-decanol (j), *n*-undecanol (k), 1,3-propanediol (l), 1,4-butanediol (m); Figure S5: CPL spectra of **DSBA** in methanol (a), ethanol (b), *n*-propanol (c), *n*-butanol (d), *n*-pentanol e), *n*-hexanol (f), *n*-heptanol (g), *n*-octanol (h), *n*-nonanol (i), *n*-decanol (j), *n*-undecanol (k), ethyleneglycol (l), 1,3-propanediol (m), 1,4-butanediol (n); Figure S6: CD spectra of **DSBA** in methanol (a), ethanol (b), *n*-propanol (c), *n*-butanol (d), *n*-pentanol (e), *n*-hexanol (f), *n*-heptanol (g), *n*-octanol (h), *n*-nonanol (i), *n*-decanol (j), *n*-undecanol (k), 1,3-propanediol (l), 1,4-butanediol (m); Figure S7: CPL spectra of **DSBP** in methanol ol (a), ethanol (b), *n*-propanol (c), *n*-butanol (d), *n*-pentanol e), *n*-hexanol (f), *n*-heptanol (g), *n*-octanol (h), *n*-nonanol (i), *n*-decanol (j), *n*-undecanol (k), ethyleneglycol (l), 1,3-propanediol (m), 1,4-butanediol (n); Figure S8: CD spectra of **DSBP** in methanol (a), ethanol (b), *n*-propanol (c), *n*-butanol (d), *n*-pentanol (e), *n*-hexanol (f), *n*-heptanol (g), *n*-octanol (h), *n*-nonanol (i), *n*-decanol (j), *n*-undecanol (k), 1,3-propanediol (l), 1,4-butanediol (m); Figure S9: CPL spectra of **BA** in methanol (a), ethanol (b), *n*-propanol (c); Figure S10: CPL spectra of **PP** in methanol (a), ethanol (b), *n*-propanol (c), *n*-butanol (d), *n*-pentanol e), *n*-hexanol (f), *n*-heptanol (g), *n*-octanol (h), *n*-nonanol (i), *n*-decanol (j), *n*-undecanol (k); Figure S11: CD spectra of **PP** in methanol (a), ethanol (b), *n*-propanol (c), *n*-butanol (d), *n*-pentanol (e), *n*-hexanol (f), *n*-heptanol (g), *n*-octanol (h), *n*-nonanol (i), *n*-decanol (j), *n*-undecanol (k), D_2O (l), Figure S11: CD spectra of **PP** in methanol (a), ethanol (b), *n*-propanol (c), *n*-butanol (d), *n*-pentanol (e), *n*-hexanol (f), *n*-heptanol (g), *n*-octanol (h), *n*-nonanol (i), *n*-decanol (j), *n*-undecanol (k), D_2O (l); Figure S12: Plot of v_a–v_f vs. $f(\varepsilon, n)$ and $v_a + v_f$ vs. $f(\varepsilon, n) + 2g(n)$ for **DSA** in various alcohols; Figure S13: Plot of v_a-v_f vs. $f(\varepsilon, n)$ and $v_a + v_f$ vs. $f(\varepsilon, n) + 2g(n)$ for **DSBA** in various alcohols; Figure S14: Plot of v_a–v_f vs. $f(\varepsilon, n)$ and $v_a + v_f$ vs. $f(\varepsilon, n) + 2g(n)$ for **DSBP** in various alcohols; Figure S15: Photographs of solid state emission of **DSA** (a), **DSBA** (b) and **DSBP** (c); Figure S16: Graph of forced dihedral angle vs. ground state energy of **BA**; Figure S17: Graph of g_{lum} vs. viscosity of the solvent for **DA** (a) and **PP** (b); Figure S18: Experimental and predicted UV-Visible spectra of **DSA** obtained with TD-DFT (B3LYP, 6-311G basis set). Table S1: Table of solvent parameters; Table S2: Table of transition dipole moment values for **DSA**, **DSBA**, and **DSBP**; Table S3: Table of K_f, Φ and τ values of **DSA** in selected solvents; Table S4: Table of K_f, Φ and τ values of **DSBA** in selected solvents; Table S5: Table of K_f, Φ_f, and τ values of **DSBP** in selected solvents; Table S6: Optimized structure, HOMO and LUMO of **DSA**, **DSBA**, and **DSBP** obtained with DFT (B3LYP functional, 6-311G basis set) using Gaussian 09 (rev D.01) and GaussView5.

Author Contributions: Three luminophores, **DSA**, **DSBA**, and **DSBP**, were synthesized and characterized by P.P. and B.N. The chiroptical properties of five luminophores (**DSA**, **DSBA**, **DSBP**, **BA**, and **PP**) were co-measured and co-verified by P.P. and M.F, who was a technical staffer at NAIST using CPL-200 and CD J820 spectrometers located in a lab of M.F. The spectrometers were routinely maintained and calibrated with ethanol solutions (0.4 wt/v) of *D*-/*L*-camphor by Yasuo Nakanishi who is a JASCO engineer. The relative quantum efficiency using 9,10-diphenylanthracene (Φ_f 0.97 in

cyclohexane) as a standard was measured and preliminarily analyzed by M.F., and P.P. Theoretical calculation obtained with Gaussian09 package was carried out by P.P. and M.F. The lifetime of PL was measured and analyzed by S.S., P.P., and B.N. The manuscript was co-written by P.P., M.F., and B.N. Requests for all original raw and processed data sets, should be sent to P.P. (puhuppuneet@gmail.com) and M.F. (fujikim@ms.naist.jp). All authors have read and agreed to the published version of the manuscript.

Funding: This research was supported by a grant from the Department of Science and Technology, India (SR/NM/NS-1439/2014).

Institutional Review Board Statement: Not applicable.

Informed Consent Statement: Not applicable.

Data Availability Statement: Data may be available on request.

Acknowledgments: P.P. is thankful to the SERB, Department of Science and Technology, India for a National Post-Doctoral Fellowship. Thanks to Seiko Amazumi (S.A.) for co-measurement and co-verification of CD and CPL spectra.

Conflicts of Interest: The authors declare no conflict of interest. The funders had no role in the design of the study; in the collection, analyses, or interpretation of data; in the writing of the manuscript, or in the decision to publish the results.

References

1. Breslow, R. A likely possible origin of homochirality in amino acids and sugars on prebiotic earth. *Tetrahedron Lett.* **2011**, *52*, 2028–2032. [CrossRef]
2. Harada, K.; Fox, S.W. Thermal Synthesis of Natural Amino-Acids from a Postulated Primitive Terrestrial Atmosphere. *Nat. Cell Biol.* **1964**, *201*, 335–336. [CrossRef] [PubMed]
3. Hanafusa, H.; Akabori, S. Polymerization of Aminoacetonitrile. *Bull. Chem. Soc. Jpn.* **1959**, *32*, 626–630. [CrossRef]
4. Miller, S.L. A Production of Amino Acids Under Possible Primitive Earth Conditions. *Science* **1953**, *117*, 528–529. [CrossRef]
5. Wigner, E. Einige Folgerungen aus der Schrödingerschen Theorie für die Termstrukturen. *Eur. Phys. J. A* **1927**, *43*, 624–652. [CrossRef]
6. Yamagata, Y. A hypothesis for the asymmetric appearance of biomolecules on earth. *J. Theor. Biol.* **1966**, *11*, 495–498. [CrossRef]
7. Rein, D.W. Some remarks on parity violating effects of intramolecular interactions. *J. Mol. Evol.* **1974**, *4*, 15–22. [CrossRef] [PubMed]
8. Letokhov, V. On difference of energy levels of left and right molecules due to weak interactions. *Phys. Lett. A* **1975**, *53*, 275–276. [CrossRef]
9. Fujiki, M. Mirror Symmetry Breaking in Helical Polysilanes: Preference between Left and Right of Chemical and Physical Origin. *Symmetry* **2010**, *2*, 1625–1652. [CrossRef]
10. Keszthelyi, L. Origin of the asymmetry of biomolecules and weak interaction. *Orig. life Evol. Biosph.* **1977**, *8*, 299–340. [CrossRef] [PubMed]
11. Harris, R.; Stodolsky, L. Quantum beats in optical activity and weak interactions. *Phys. Lett. B* **1978**, *78*, 313–317. [CrossRef]
12. Hegstrom, R.A.; Rein, D.W.; Sandars, P.G.H. Calculation of the parity nonconserving energy difference between mirror-image molecules. *J. Chem. Phys.* **1980**, *73*, 2329–2341. [CrossRef]
13. Mason, S.F.; Tranter, G.E. Energy inequivalence of peptide enantiomers from parity non-conservation. *J. Chem. Soc. Chem. Commun.* **1983**, 117–119. [CrossRef]
14. Mason, S.; Tranter, G. The parity-violating energy difference between enantiomeric molecules. *Mol. Phys.* **1984**, *53*, 1091–1111. [CrossRef]
15. Barron, L.D. Symmetry and molecular chirality. *Chem. Soc. Rev.* **1986**, *15*, 189–223. [CrossRef]
16. Quack, M. Structure and Dynamics of Chiral Molecules. *Angew. Chem. Int. Ed.* **1989**, *28*, 571–586. [CrossRef]
17. Hegstrom, R.A.; Kondepudi, D.K. The Handedness of the Universe. *Sci. Am.* **1990**, *262*, 108–115. [CrossRef]
18. Salam, A. The role of chirality in the origin of life. *J. Mol. Evol.* **1991**, *33*, 105–113. [CrossRef]
19. MacDermott, A.J. Electro weak enantioselection and the origin of life. *Orig. Life Evol. Biosph.* **1995**, *25*, 191–199. [CrossRef]
20. Kikuchi, O.; Kiyonaga, H. Parity-violating energy shift of helical n-alkanes. *J. Mol. Struct. Theochem.* **1994**, *312*, 271–274. [CrossRef]
21. Avetisov, V.; Goldanskii, V. Mirror symmetry breaking at the molecular level. *Proc. Natl. Acad. Sci. USA* **1996**, *93*, 11435–11442. [CrossRef] [PubMed]
22. Bonner, W.A. Enantioselective autocatalysis. IV. Implications for parity violation effects. *Orig. Life Evol. Biosph.* **1996**, *26*, 27–45. [CrossRef]
23. Szabó-Nagy, A.; Keszthelyi, L. Demonstration of the parity-violating energy difference between enantiomers. *Proc. Natl. Acad. Sci. USA* **1999**, *96*, 4252–4255. [CrossRef]
24. Compton, R.N.; Pagni, R.M. The Chirality of Biomolecules. *Adv. At. Mol. Opt. Phys.* **2002**, *48*, 219–261. [CrossRef]

25. Schwerdtfeger, P.; Gierlich, J.; Bollwein, T. Large Parity-Violation Effects in Heavy-Metal-Containing Chiral Compounds. *Angew. Chem. Int. Ed.* **2003**, *42*, 1293–1296. [CrossRef]
26. MacDermott, A.; Hegstrom, R. A proposed experiment to measure the parity-violating energy difference between enantiomers from the optical rotation of chiral ammonia-like "cat" molecules. *Chem. Phys.* **2004**, *305*, 55–68. [CrossRef]
27. Quack, M.; Stohner, J.; Willeke, M. High-Resolution Spectroscopic Studies and Theory of Parity Violation in Chiral Molecules. *Annu. Rev. Phys. Chem.* **2008**, *59*, 741–769. [CrossRef]
28. Bargueño, P.; Gonzalo, I.; De Tudela, R.P.; Gonzalo, I. Detection of parity violation in chiral molecules by external tuning of electroweak optical activity. *Phys. Rev. A* **2009**, *80*. [CrossRef]
29. Dorta-Urra, A.; Peñate-Rodríguez, H.C.; Bargueño, P.; Rojas-Lorenzo, G.; Miret-Artés, S. Dissipative geometric phase and decoherence in parity-violating chiral molecules. *J. Chem. Phys.* **2012**, *136*, 174505. [CrossRef]
30. Famiano, M.A.; Boyd, R.N.; Kajino, T.; Onaka, T.; Mo, Y. Amino Acid Chiral Selection Via Weak Interactions in Stellar Environments: Implications for the Origin of Life. *Sci. Rep.* **2018**, *8*, 8833. [CrossRef]
31. Daussy, C.; Marrel, T.; Amy-Klein, A.; Nguyen, C.T.; Bordé, C.J.; Chardonnet, C. Limit on the Parity Nonconserving Energy Difference between the Enantiomers of a Chiral Molecule by Laser Spectroscopy. *Phys. Rev. Lett.* **1999**, *83*, 1554–1557. [CrossRef]
32. Lee, T.D.; Yang, C.N. Question of Parity Conservation in Weak Interactions. *Phys. Rev.* **1956**, *104*, 254–258. [CrossRef]
33. Wu, C.S.; Ambler, E.; Hayward, R.W.; Hoppes, D.D.; Hudson, R.P. Experimental Test of Parity Conservation in Beta Decay. *Phys. Rev.* **1957**, *105*, 1413–1415. [CrossRef]
34. Quantum Systems in Chemistry and Physics. *Concepts Methods Appl. Quantum Syst. Chem. Phys.* **2012**, *26*, 47–76. [CrossRef]
35. Quack, M. How Important is Parity Violation for Molecular and Biomolecular Chirality? *Angew. Chem. Int. Ed.* **2002**, *41*, 4618–4630. [CrossRef]
36. Soncini, A.; Faglioni, F.; Lazzeretti, P. Parity-violating contributions to nuclear magnetic shielding. *Phys. Rev. A* **2003**, *68*, 033402. [CrossRef]
37. Arimondo, E.; Glorieux, P.; Oka, T. Observation of inverted infrared lamb dips in separated optical isomers. *Opt. Commun.* **1977**, *23*, 369–372. [CrossRef]
38. Crassous, J.; Monier, F.; Dutasta, J.-P.; Ziskind, M.; Daussy, C.; Grain, C.; Chardonnet, C. Search for Resolution of Chiral Fluorohalogenomethanes and Parity-Violation Effects at the Molecular Level. *Chem. Phys. Chem.* **2003**, *4*, 541–548. [CrossRef] [PubMed]
39. Lahamer, A.S.; Mahurin, S.M.; Compton, R.N.; House, D.; Laerdahl, J.K.; Lein, M.; Schwerdtfeger, P. Search for a Parity-Violating Energy Difference between Enantiomers of a Chiral Iron Complex. *Phys. Rev. Lett.* **2000**, *85*, 4470–4473. [CrossRef]
40. Robert, J.-B.; Barra, A. NMR and parity nonconservation. Experimental requirements to observe a difference between enantiomer signals. *Chirality* **2001**, *13*, 699–702. [CrossRef]
41. Darquié, B.; Stoeffler, C.; Shelkovnikov, A.; Daussy, C.; Amy-Klein, A.; Chardonnet, C.; Zrig, S.; Guy, L.; Crassous, J.; Soulard, P.; et al. Progress toward the first observation of parity violation in chiral molecules by high-resolution laser spectroscopy. *Chirality* **2010**, *22*, 870–884. [CrossRef] [PubMed]
42. Fujiki, M.; Koe, J.R.; Mori, T.; Kimura, Y. Questions of Mirror Symmetry at the Photoexcited and Ground States of Non-Rigid Luminophores Raised by Circularly Polarized Luminescence and Circular Dichroism Spectroscopy: Part 1. Oligofluorenes, Oligophenylenes, Binaphthyls and Fused Aromatics. *Molecules* **2018**, *23*, 2606. [CrossRef]
43. Fujiki, M.; Koe, J.R.; Amazumi, S. Questions of Mirror Symmetry at the Photoexcited and Ground States of Non-Rigid Luminophores Raised by Circularly Polarized Luminescence and Circular Dichroism Spectroscopy. Part 2: Perylenes, BODIPYs, Molecular Scintillators, Coumarins, Rhodamine B, and DCM. *Symmetry* **2019**, *11*, 363. [CrossRef]
44. Norrgard, E.B.; Barker, D.S.; Eckel, S.; Fedchak, J.A.; Klimov, N.N.; Scherschligt, J. Nuclear-spin dependent parity violation in optically trapped polyatomic molecules. *Commun. Phys.* **2019**, *2*, 1–6. [CrossRef]
45. Eills, J.; Blanchard, J.W.; Bougas, L.; Kozlov, M.G.; Pines, A.; Budker, D. Measuring molecular parity nonconservation using nuclear-magnetic-resonance spectroscopy. *Phys. Rev. A* **2017**, *96*, 042119. [CrossRef]
46. Sang, Y.; Liu, M. Symmetry Breaking in Self-Assembled Nanoassemblies. *Symmetry* **2019**, *11*, 950. [CrossRef]
47. Emeis, C.; Oosterhoff, L. Emission of circularly-polarised radiation by optically-active compounds. *Chem. Phys. Lett.* **1967**, *1*, 129–132. [CrossRef]
48. Ribó, J.M.; Hochberg, D.; Crusats, J.; El-Hachemi, Z.; Moyano, A. Spontaneous mirror symmetry breaking and origin of biological homochirality. *J. R. Soc. Interface* **2017**, *14*, 20170699. [CrossRef]
49. Ribó, J.M.; Hochberg, D. Chemical Basis of Biological Homochirality during the Abiotic Evolution Stages on Earth. *Symmetry* **2019**, *11*, 814. [CrossRef]
50. He, J.; Xu, B.; Chen, F.; Xia, H.; Li, K.; Ye, L.; Tian, W. Aggregation-Induced Emission in the Crystals of 9,10-Distyrylanthracene Derivatives: The Essential Role of Restricted Intramolecular Torsion. *J. Phys. Chem. C* **2009**, *113*, 9892–9899. [CrossRef]
51. Ii, G.J.; Jackson, W.R.; Choi, C.Y.; Bergmark, W.R. Solvent effects on emission yield and lifetime for coumarin laser dyes. Requirements for a rotatory decay mechanism. *J. Phys. Chem.* **1985**, *89*, 294–300. [CrossRef]
52. Nadaf, Y.; Mulimani, B.; Gopal, M.; Inamdar, S. Ground and excited state dipole moments of some exalite UV laser dyes from solvatochromic method using solvent polarity parameters. *J. Mol. Struct. Theochem.* **2004**, *678*, 177–181. [CrossRef]
53. Kozlova, S.; Gabuda, S.P. Thermal properties of Zn2(C8H4O4)2•C6H12N2 metal-organic framework compound and mirror symmetry violation of dabco molecules. *Sci. Rep.* **2017**, *7*, 11505. [CrossRef]

54. Quack, M. On the measurement of the parity violating energy difference between enantiomers. *Chem. Phys. Lett.* **1986**, *132*, 147–153. [CrossRef]
55. Berger, R. Molecular parity violation in electronically excited states. *Phys. Chem. Chem. Phys.* **2002**, *5*, 12–17. [CrossRef]
56. Bouchiat, M.-A.; Pottier, L.; Howard, R.E.; Jackel, L.D.; Mankiewich, P.M.; Skocpol, W.J. Optical Experiments and Weak Interactions. *Science* **1986**, *234*, 1203–1210. [CrossRef] [PubMed]
57. Wang, W.; Yi, F.; Ni, Y.; Zhao, Z.; Jin, X.; Tang, Y. Parity Violation of Electroweak Force in Phase Transitions of Single Crystals of D- and L-Alanine and Valine. *J. Biol. Phys.* **2000**, *26*, 51–65. [CrossRef] [PubMed]
58. Pagni, R.M.; Compton, R.N. Asymmetric Synthesis of Optically Active Sodium Chlorate and Bromate Crystals. *Cryst. Growth Des.* **2002**, *2*, 249–253. [CrossRef]
59. Scolnik, Y.; Portnaya, I.; Cogan, U.; Tal, S.; Haimovitz, R.; Fridkin, M.; Elitzur, A.C.; Deamer, D.W.; Shinitzky, M. Subtle differences in structural transitions between poly-l- and poly-d-amino acids of equal length in water. *Phys. Chem. Chem. Phys.* **2005**, *8*, 333–339. [CrossRef]
60. Kodona, E.K.; Alexopoulos, C.; Panou-Pomonis, E.; Pomonis, P.J. Chirality and helix stability of polyglutamic acid enantiomers. *J. Colloid Interface Sci.* **2008**, *319*, 72–80. [CrossRef]
61. Albert, S.; Arn, F.; Bolotova, I.; Chen, Z.; Fábri, C.; Grassi, G.; Lerch, P.; Quack, M.; Seyfang, G.; Wokaun, A.; et al. Synchrotron-Based Highest Resolution Terahertz Spectroscopy of the ν24Band System of 1,2-Dithiine (C4H4S2): A Candidate for Measuring the Parity Violating Energy Difference between Enantiomers of Chiral Molecules. *J. Phys. Chem. Lett.* **2016**, *7*, 3847–3853. [CrossRef] [PubMed]
62. Inamdar, S.; Nadaf, Y.; Mulimani, B. Ground and excited state dipole moments of exalite 404 and exalite 417 UV laser dyes determined from solvatochromic shifts of absorption and fluorescence spectra. *J. Mol. Struct. Theochem.* **2003**, *624*, 47–51. [CrossRef]